Metal-Organic Framework Templated Synthesis of Ultrathin, Well-Aligned Metallic Nanowires

Boris Volosskiy,[†] Kenta Niwa,[†] Yu Chen,[‡] Zipeng Zhao,[‡] Nathan O. Weiss,[‡] Xing Zhong,[†] Mengning Ding,[‡] Chain Lee,[†] Yu Huang,[‡,§] and Xiangfeng Duan[*,†,§]

[†]Department of Chemistry and Biochemistry, [‡]Department of Materials Science and Engineering, and [§]California Nanosystems Institute, University of California, Los Angeles, Los Angeles, California 90095, United States

ABSTRACT With well-defined porous structures and dimensions, metal-organic frameworks (MOFs) can function as versatile templates for the growth of metallic nanostructures with precisely controlled shapes and sizes. Using MOFs as templates, metallic nanostructures can be grown without the need of bulky surfactants and thus preserve their intrinsic surface. Additionally, the high surface area of MOFs can also ensure that the surface of the template metallic nanostructures is readily accessible, which is critical for the proper function of catalysts or sensors. The hybrid metal@MOF structures have been demonstrated to exhibit useful properties not found in either component separately. Here we report the growth of ultrafine metallic nanowires inside one-dimensional MOF pores with well-controlled shape and size. Our study shows that solvent selection plays an important role in controlling precursor loading and the reduction rate inside the MOF pores for the formation of the nanowires. The growth of the well-aligned, ultrathin nanowires was monitored and characterized by transmission electron microscopy, X-ray diffraction, UV–vis spectroscopy, fluorescence studies, and Brunauer–Emmet–Teller surface area analysis.

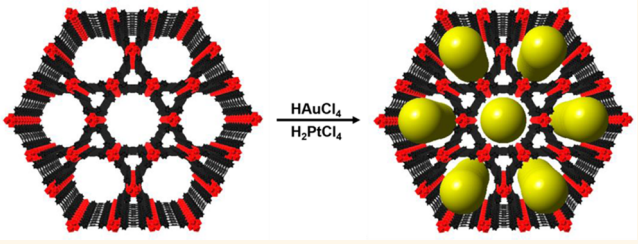

KEYWORDS: metal–organic frameworks · nanoparticles · nanowires · host–guest systems

Metal-organic frameworks (MOFs) have emerged as a new class of porous, multifunctional materials with great variations in their structures and properties. To date, the research efforts on MOFs have been primarily focusing on the synthesis of new structures for general applications in gas storage and separation.[1−4] More recently, other properties and applications have been explored including catalysis, sensing, and as components for the synthesis of hybrid materials.[5−12] In particular, there have been numerous reports of noble metal nanoparticles and MOF hybrids (metal@MOF) for a variety of applications. Furukawa and co-workers reported the synthesis of a MOF shell around previously synthesized Au nanorods, which they used for photothermal gas release.[13] Huo *et al.* reported similar growth of a zeolitic imidazolate framework (ZIF) around a variety of noble metal nanostructures, which were characterized for optical and catalytic applications.[14] These two reports are just a few of the recent examples in this rapidly growing field due to the interesting properties and promising applications of these hybrid materials.[15−23] Despite the increasing reports in the past few years, there are none that emphasize synthetic possibilities of using pore dimension to control the shape and size of the resulting nanostructures.

Extensive research has been conducted on controlling the shape and size of metal nanostructures due to their unique plasmonic resonance, catalytic behavior, and sensing ability, among many other promising applications.[24,25] A variety of metallic nanostructures of different shapes and sizes have been synthesized. Challenges still remain in fully controlling the dimensions and morphologies of these nanostructures, as well as maximizing the exposure of the active surfaces.[26,27] By using surfactants or selected capping ligands, the shape and size can often be precisely controlled, but the capping ligands limit the accessibility of the surface. A potential solution to this challenge

* Address correspondence to xduan@chem.ucla.edu.

Received for review December 18, 2014 and accepted February 21, 2015.

Published online February 22, 2015
10.1021/nn5072446

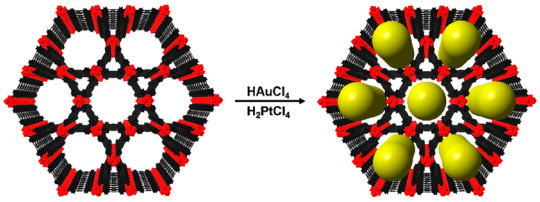

Figure 1. Model of MOF-545 with 1D pores as templates for the synthesis of well-aligned nanowires.

is to use a template that confines the growth of the nanostructures. This can prevent aggregation, control the shape and size, and allow for a large percentage of exposed metallic surface due to the absence of surfactants. An ideal template should have nanosized pores that could easily be modified to display a variety of shapes and sizes, as well as maintain its structure in a multitude of conditions. High surface area is also optimal to allow access to the resulting nanostructures, without having to dissolve away the template.[28] Importantly, MOFs fit all these requirements and furthermore have also been shown to exhibit synergistic effects and properties. The hybrid nanoparticles@MOF materials have been shown to display unique catalytic, sensing, and chemi- and physisorption capabilities not found in either nanoparticles or MOFs alone.[29−33]

There have been previous reports of growing nanoparticles inside 3D MOFs, but to the best of our knowledge, there is no report that uses one-dimensional (1D) MOF pores to grow 1D nanostructures. Here we demonstrate the first example of using 1D-channel MOF pores to synthesize well-aligned Au and Pt nanowires with the dimensions determined by the size of MOF pores. Figure 1 schematically illustrates the formation of well-defined metallic nanowires inside the 1D pores of the MOF-545 template. MOF-545 contains cubic $Zr_6O_8(CO_2)_8(H_2O)_8$ as the secondary building units, which are connected by four-coordinated tetrakis(4-carboxyphenyl)porphyrin (TCPP) linkers. These two components form a hexagonal framework with unit cell parameters of $a = 42.545$ Å and $c = 16.96$ Å.[34] MOF-545 features channel-like pores along its c-axis with a channel periodicity of 37 Å. Considering the out-of-plane benzene rings, bulky zirconium clusters, and solvent molecules around the clusters, the inner diameter of the channel is expected to be approximately 30 Å (Figure S1).

RESULTS

The MOF-545 template was prepared using a previously reported method,[34] and its structure was confirmed by powder X-ray diffraction (PXRD). The most prominent diffraction peaks at 36.9 Å and 18.5 Å correspond to the (010) and (020) lattice spacing of the MOF-545 crystals (Figure 2a). The morphology of the as-synthesized MOF was characterized using transmission electron microscopy (TEM) (Figure 2b−d). In general, the MOF crystals exhibit a wire-like morphology (Figure 2b and inset). The high-magnification TEM

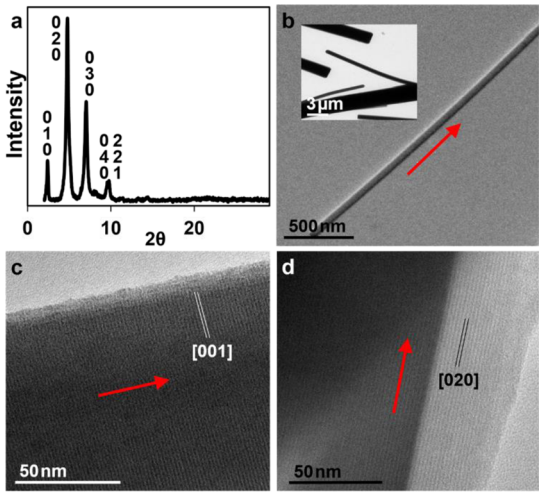

Figure 2. Characterization of the as-synthesized MOF. (a) PXRD of the as-synthesized MOF-545. (b) Low-magnification TEM image of the MOF, showing wire-like morphology. The inset shows a lower magnification image with multiple MOF wires. (c) High-magnification TEM image showing (001) lattice fringes perpendicular to the MOF wire axis. (d) Low-magnification TEM image showing (020) lattice fringes parallel to the MOF wire axis. The red arrows indicate the MOF wire axis direction.

images show clear lattice fringes perpendicular and parallel to the nanowire axis, which can be mistaken as the pore channels at first glance (Figure 2c, 2d). A careful analysis of the high-magnification TEM images reveals a line spacing of 1.65 nm (Figure 2c) and 1.85 nm (Figure 2d), respectively. Upon further analysis of these gratings in a high-resolution TEM image and its fast Fourier transform (FFT) (Figure S2), the 1.85 nm distance seen in Figure 2d corresponds to the spacing between (020) lattice planes. The 1.65 nm spacing that can be seen perpendicular to the MOF nanowire axis corresponds to the (001) direction (Figure 2c).

It was hypothesized that the growth of the nanowires inside the MOF pores required the metallic precursor solution to favorably diffuse inside. Once the metal ions are within the MOF pores, optimal nucleation and growth rates are crucial to obtain dense nanowire arrays throughout the MOF. The ideal reduction conditions would prevent excessive growth that could lead to MOF breakdown, while still allowing the formation of long nanowires. To this end, the solvent and reducing agent are critical. To discover the best solvent system, we attempted loading and reducing gold chloride in a series of solvents, including water, acetone, hexane, acetic acid, and sodium hydroxide. The reaction solution was prepared by dissolving 9 mg of gold chloride hydrate in 10 mL of solvent, and 0.5 mg of MOF-545 was added to the mixture. The vial was capped and allowed to react at 35 °C for 14 h.

In general, because of the polar nature of MOF-545 crystals, the MOF particles cannot be dispersed well in nonpolar solvents such as hexane, and consequently, no gold nanoparticles were observed in the MOF pores

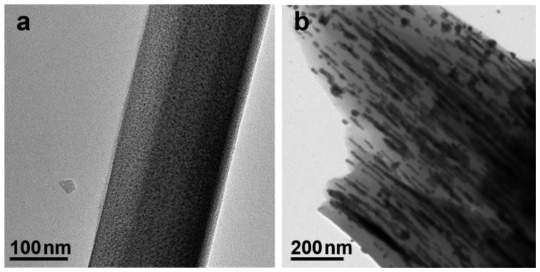

Figure 3. MOF-545 as a template for the nucleation and growth of Au nanoparticles. (a) TEM image showing the high density of small Au particles, synthesized by low heating of Au precursor in acetone. (b) TEM image of samples synthesized in water, displaying nanorods and wires in high density with diameters on average of ~10 nm.

or on the MOF surface. In the case of acetone solution, a high density of high-contrast Au nanoparticles were seen in the MOF crystals (Figure 3a), suggesting that gold chloride dissolved in acetone can readily diffuse into the MOF pores and favorably interact with the MOF-545 template. The observation of nanoparticles inside the MOF pores confirms the presence of precursor inside the MOF, but there is an apparent lack of elongation. The lack of growth along the longitudinal direction of the pores is likely due to the absence of a reducing agent and very high [H^+] concentration (from the strong acidic nature of the gold chloride hydrate precursor), conditions in which gold chloride may not be readily reduced.

Interestingly, the reactions in water produced a large number of elongated nanowires inside the MOF crystal (Figure 3b). It is evident from the TEM image that the Au nanowires exhibit a variable diameter distribution with an average around 10 nm. This diameter is considerably larger than the expected value based on the 3.0 nm pore diameter in the MOF crystals, which suggests partial breakdown of the MOF crystal. Structural analysis by XRD reveals expected MOF-545 diffraction peaks and the appearance of Au peaks (Figure S3), suggesting that the overall MOF-545 structure is maintained despite the partial breakdown during formation of larger Au nanowires.

As compared with acetone, the reactions in water had much lower [H^+] with an initial pH of 3.1. It has been previously suggested that the redox potential of gold chloride increases with pH.[35−37] Therefore, with decreasing [H^+] concentration and increasing pH, it is not a surprise to see more gold chloride reduction and gold nanoparticle formation. We have further investigated the dependence of the MOF stability and gold aggregation based on pH by conducting the reaction in 0.001 M NaOH with an initial pH of 7.7. These reactions showed very large aggregates with no apparent shape and excessive MOF breakdown, confirming the increased reduction and MOF breakdown under high-pH conditions.

Finally, the samples prepared in 0.5 M acetic acid show a high density of ultrathin, well-aligned nanowires

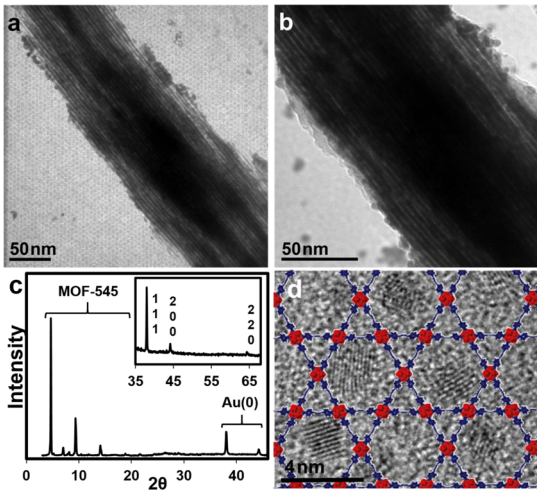

Figure 4. Au nanowire formation in MOF-545 in 0.5 M glacial acetic acid. (a, b) TEM image showing long, thin, aligned nanowires with 2−3 nm diameters at (a) lower and (b) higher magnifications. (c) XRD of Au@MOF-545 using acetic acid solvent system, showing retention of the MOF structure and confirming Au(0) formation. (d) TEM images with the hexagonal MOF template showing the cross section of the MOF and Au wires.

with diameters of 2−3 nm (Figure 4). The results seen in this system can be attributed to the presence of acetic acid as a weak reducing agent as compared to the system with just water. The reactions done in acetic acid were measured to have an initial pH of 2.95, very similar to the pH of 3.10 observed in water. The presence of acetic acid as a reducing agent likely promotes more nucleation, which in turn limits the amount of precursor left for elongation and growth. The slightly lower pH may enhance MOF stability and thus lead to the formation of highly uniform nanowire arrays defined by the MOF pore dimension. Further evidence can be seen when comparing the densities of wires synthesized in water to those synthesized in acetic acid. It is evident that there is a much higher density of thinner nanowires in the acetic acid system (Figure 4), as compared to lower densities of larger nanowires in water (Figure 3b). Figure 4c shows the XRD data of the samples synthesized in acetic acid, confirming the retention of the MOF structure and appearance of gold peaks (Figure 4c inset).

The high densities of wires make it rather challenging to image individual nanowires due to significant overlap and limited contrast, especially toward the center of the MOF wire. To further confirm the presence of the gold nanowires inside the MOF pores, we prepared a cross-section sample using focused ion beam (FIB) cutting and analyzed the sample by TEM imaging (Figure 4d). The TEM image showed that the cross section of the MOF contains a high density of round Au cross sections. Furthermore, it is apparent that the Au nanowire cross sections fit into a hexagonal structure of the MOF template. The optical properties of the Au@MOF samples containing the ultrathin nanowires were characterized using fluorescence measurements and UV−vis

(Figures S4, S5). The UV−vis showed a shift of the S and Q-band peaks, consistent with the formation of Au(III) TCPP.[38,39] The small 2−3 nm diameter of the gold nanowires and the presence of the porphyrin-MOF shell highly limit the relative intensity of the transverse plasmon resonance and make it nearly impossible to isolate the plasmon resonance peak from the Q-band at 535 nm.[38,39] The fluorescence of the Au@MOF samples was quenched (Figure S4) and can be attributed to the formation of the Au(III)TCPP complex and quenching by the gold nanowires.[38−42]

The above studies clearly demonstrate that MOF crystals can function as a robust template for the synthesis of ultrafine nanowires with precisely controlled diameter. To further show that this is a general strategy that can be extended to a wide variety of materials, we have used MOF-545 as the template to prepare Pt nanowires. At first, the same synthetic system was attempted; a 0.5 M acetic acid solution containing platinum chloride hydrate was added to MOF-545. The initial reactions led to very high densities of particles (Figure S6), very similar to the results seen with gold in acetone. These results were consistent since Pt(II)/Pt has a lower redox potential (E° = 1.19 V) than Au(III)/Au (E° = 1.54 V) and therefore would require a stronger reducing environment to mimic the same reduction and nucleation rates used for gold. To this end, we have used a stronger reducing environment (formic acid in ethylene glycol) to successfully obtain a high density of ultrathin, well-aligned Pt nanowires with diameters of 2−3 nm (Figure 5a,b) in MOF-545. We have also investigated the Pt@MOF material using cross-sectional TEM images. The lower magnification TEM showed a high density of nanowires throughout the cross section (Figure 5c), displaying hexagonal symmetry with a periodicity of 4.2 nm (see FFT in inset in Figure 5c). The high magnification images were overlaid by the MOF-545 model (Figure 5d), further demonstrating the expected hexagonal array.

The Pt@MOF-545 samples were also characterized by fluorescence measurements, UV−vis, XRD, and Brunauer−Emmet−Teller (BET) surface area measurements (Figures S4, S5, S7, and S8). The fluorescence measurements showed the same type of quenching behavior as seen in Au@MOF-545 samples. The UV−vis spectra showed the overall peak structure of MOF-545 and TCPP. Surface area measurements were performed on both Pt@MOF-545 and Au@MOF-545 samples, as well as a bare MOF-545 template. MOF-545 was measured to have a BET surface area of 2200 m^2/g, comparable to the previous reports.[34] The BET surface area of

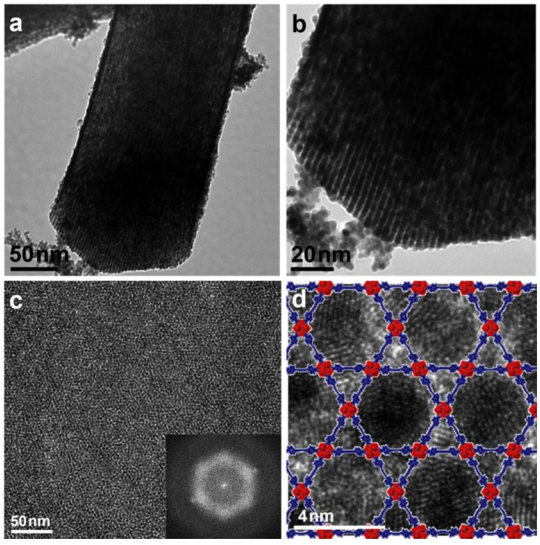

Figure 5. Pt nanowire formation in MOF-545 in ethylene glycol and formic acid. (a) TEM images showing long, thin, aligned nanowires with 2−3 nm diameters. (b) Higher magnification TEM image of the same area seen in (a). (c) TEM image showing a low-magnification cross section with nanowire growth in the hexagonal lattice as seen by the FFT. (d) Higher magnification TEM image showing the hexagonal model of the MOF fitted over the cross section.

Au@MOF-545 or Pt@MOF-545 samples ranged from 100 to 400 m^2/g, depending on the amount of metal loaded. The reduction of specific surface area is partly attributed to the mass increase upon loading with Au or Pt.

CONCLUSION

In summary, we have demonstrated the first successful synthesis of metal nanostructures in which the shape of the MOF pore controls both the morphologies and dimensions of the nanostructures. The nanostructures grown inside the MOF do not have long-chain surfactants on them, and the high surface area of the MOF allows for easy access to the surface. In addition, the hybrid nanostructures@MOF can be directly used for catalysis, without having to put the particles on other substrates postsynthesis. MOFs not only can serve as templates and supports but also can be modified to enhance or assist the properties and applications of the nanostructures. The presence of porphyrin active sites, high surface area, plasmonic gold nanowires, or highly active platinum nanowires offers a powerful combination of highly distinct properties, opening up exciting opportunities for many applications. Notably, the system reported here offers great potential and is currently being investigated as a synergistic catalyst for a variety of reactions.

METHODS

Au@MOF-545 in acetone/water/hexane: 9 mg of gold chloride hydrate $HAu(III)Cl_4$ was dissolved in 10 mL of acetone/water/hexane. A 0.5 mg amount of MOF-545 was added to the solution, and the capped vial was briefly sonicated and allowed to react for 14 h at 35 °C. The MOF was then exchanged with acetone three times to wash away any unreacted precursor.

Au@MOF-545 in NaOH: 9 mg of gold chloride hydrate HAu(III)Cl_4 was dissolved in 9.6 mL of water and 2.5 mg of NaOH. A 0.5 mg amount of MOF-545 was added to the solution, and the capped vial was briefly sonicated and allowed to react for 14 h at 35 °C. The MOF was then exchanged with water and acetone three times to wash away any unreacted precursor.

Au@MOF-545 in sodium acetate: 9 mg of gold chloride hydrate HAu(III)Cl_4 was dissolved in 9.6 mL of water and 20 mg of sodium acetate. A 0.5 mg amount of MOF-545 was added to the solution, and the capped vial was briefly sonicated and allowed to react for 14 h at 35 °C. The MOF was then exchanged with water and acetone three times to wash away any unreacted precursor.

Au@MOF-545 in acetic acid: 9 mg of gold chloride hydrate HAu(III)Cl_4 was dissolved in 9.6 mL of water and 0.4 mL of glacial acetic acid. A 0.5 mg amount of MOF-545 was added to the solution, and the capped vial was briefly sonicated and allowed to react for 14 h at 35 °C. The MOF was then exchanged with water and acetone three times to wash away any unreacted precursor.

Pt@MOF-545 in acetic acid: 7 mg of platinum chloride hydrate H_2Pt(II)Cl_4 was dissolved in 9.6 mL of water and 0.4 mL of glacial acetic acid. A 0.5 mg amount of MOF-545 was added to the solution, and the capped vial was briefly sonicated and allowed to react for 14 h at 35 °C. The MOF was then exchanged with water and acetone three times to wash away any unreacted precursor.

Pt@MOF-545 in EG/formic acid: 7 mg of platinum chloride hydrate H_2Pt(II)Cl_4 was dissolved in 9.6 mL of ethylene glycol and 0.4 mL of formic acid. A 0.5 mg amount of MOF-545 was added to the solution, and the capped vial was briefly sonicated and allowed to react for 14 h at 30 °C. The MOF was then exchanged with water and acetone three times to wash away any unreacted precursor.

Conflict of Interest: The authors declare no competing financial interest.

Supporting Information Available: Additional figures. This material is available free of charge *via* the Internet at http://pubs.acs.org.

Acknowledgment. We acknowledge the support from the U.S. Department of Energy, Office of Basic Energy Sciences, Division of Materials Science and Engineering, through Award DE-SC0008055. We thank N. Bodzin for his support in making FIB cross sections. We thank EICN at CNSI for the TEM support.

REFERENCES AND NOTES

1. Eddaoudi, M.; Kim, J.; Rosi, N.; Vodak, D.; Wachter, J.; O'Keeffe, M.; Yaghi, O. M. Systematic Design of Pore Size and Functionality in Isoreticular MOFs and Their Application in Methane Storage. *Science* **2002**, *295*, 469–472.
2. Kitagawa, S.; Kitaura, R.; Noro, S.-i. Functional Porous Coordination Polymers. *Angew. Chem., Int. Ed.* **2004**, *43*, 2334–2375.
3. Hayashi, H.; Cote, A. P.; Furukawa, H.; O'Keeffe, M.; Yaghi, O. M. Zeolite A Imidazolate Frameworks. *Nat. Mater.* **2007**, *6*, 501–506.
4. Britt, D.; Tranchemontagne, D.; Yaghi, O. M. Metal-Organic Frameworks with High Capacity and Selectivity for Harmful Gases. *Proc. Natl. Acad. Sci. U.S.A.* **2008**, *105*, 11623–11627.
5. Li, Y.; Zhang, S.; Song, D. A Luminescent Metal–Organic Framework as a Turn-On Sensor for DMF Vapor. *Angew. Chem.* **2013**, *125*, 738–741.
6. Wu, C.-D.; Hu, A.; Zhang, L.; Lin, W. A Homochiral Porous Metal–Organic Framework for Highly Enantioselective Heterogeneous Asymmetric Catalysis. *J. Am. Chem. Soc.* **2005**, *127*, 8940–8941.
7. Lee, J.; Farha, O. K.; Roberts, J.; Scheidt, K. A.; Nguyen, S. T.; Hupp, J. T. Metal-Organic Framework Materials as Catalysts. *Chem. Soc. Rev.* **2009**, *38*, 1450–1459.
8. Lin, W.; Rieter, W. J.; Taylor, K. M. L. Modular Synthesis of Functional Nanoscale Coordination Polymers. *Angew. Chem., Int. Ed.* **2009**, *48*, 650–658.
9. Imaz, I.; Hernando, J.; Ruiz-Molina, D.; Maspoch, D. Metal–Organic Spheres as Functional Systems for Guest Encapsulation. *Angew. Chem., Int. Ed.* **2009**, *48*, 2325–2329.
10. Oh, M.; Mirkin, C. A. Chemically Tailorable Colloidal Particles from Infinite Coordination Polymers. *Nature* **2005**, *438*, 651–654.
11. Uemura, T.; Yanai, N.; Kitagawa, S. Polymerization Reactions in Porous Coordination Polymers. *Chem. Soc. Rev.* **2009**, *38*, 1228–1236.
12. Seo, J. S.; Whang, D.; Lee, H.; Jun, S. I.; Oh, J.; Jeon, Y. J.; Kim, K. A Homochiral Metal-Organic Porous Material for Enantioselective Separation and Catalysis. *Nature* **2000**, *404*, 982–986.
13. Khaletskaya, K.; Reboul, J.; Meilikhov, M.; Nakahama, M.; Diring, S.; Tsujimoto, M.; Isoda, S.; Kim, F.; Kamei, K.-i.; Fischer, R. A.; *et al.* Integration of Porous Coordination Polymers and Gold Nanorods into Core–Shell Mesoscopic Composites toward Light-Induced Molecular Release. *J. Am. Chem. Soc.* **2013**, *135*, 10998–11005.
14. Lu, G.; Li, S.; Guo, Z.; Farha, O. K.; Hauser, B. G.; Qi, X.; Wang, Y.; Wang, X.; Han, S.; Liu, X.; *et al.* Imparting Functionality to a Metal–Organic Framework Material by Controlled Nanoparticle Encapsulation. *Nat. Chem.* **2012**, *4*, 310–316.
15. Zhu, Q.-L.; Li, J.; Xu, Q. Immobilizing Metal Nanoparticles to Metal–Organic Frameworks with Size and Location Control for Optimizing Catalytic Performance. *J. Am. Chem. Soc.* **2013**, *135*, 10210–10213.
16. Wei, Y.; Han, S.; Walker, D. A.; Fuller, P. E.; Grzybowski, B. A. Nanoparticle Core/Shell Architectures within MOF Crystals Synthesized by Reaction Diffusion. *Angew. Chem., Int. Ed.* **2012**, *51*, 7435–7439.
17. Moon, H. R.; Kim, J. H.; Suh, M. P. Redox-Active Porous Metal–Organic Framework Producing Silver Nanoparticles from AgI Ions at Room Temperature. *Angew. Chem., Int. Ed.* **2005**, *44*, 1261–1265.
18. El-Shall, M. S.; Abdelsayed, V.; Khder, A. E. R. S.; Hassan, H. M. A.; El-Kaderi, H. M.; Reich, T. E. Metallic and Bimetallic Nanocatalysts Incorporated into Highly Porous Coordination Polymer MIL-101. *J. Mater. Chem.* **2009**, *19*, 7625–7631.
19. Aijaz, A.; Karkamkar, A.; Choi, Y. J.; Tsumori, N.; Rönnebro, E.; Autrey, T.; Shioyama, H.; Xu, Q. Immobilizing Highly Catalytically Active Pt Nanoparticles inside the Pores of Metal–Organic Framework: A Double Solvents Approach. *J. Am. Chem. Soc.* **2012**, *134*, 13926–13929.
20. Meilikhov, M.; Yusenko, K.; Esken, D.; Turner, S.; Van Tendeloo, G.; Fischer, R. A. Metals@MOFs – Loading MOFs with Metal Nanoparticles for Hybrid Functions. *Eur. J. Inorg. Chem.* **2010**, *2010*, 3701–3714.
21. Aijaz, A.; Akita, T.; Tsumori, N.; Xu, Q. Metal–Organic Framework-Immobilized Polyhedral Metal Nanocrystals: Reduction at Solid–Gas Interface, Metal Segregation, Core–Shell Structure, and High Catalytic Activity. *J. Am. Chem. Soc.* **2013**, *135*, 16356–16359.
22. Hermes, S.; Schröter, M.-K.; Schmid, R.; Khodeir, L.; Muhler, M.; Tissler, A.; Fischer, R. W.; Fischer, R. A. Metal@MOF: Loading of Highly Porous Coordination Polymers Host Lattices by Metal Organic Chemical Vapor Deposition. *Angew. Chem., Int. Ed.* **2005**, *44*, 6237–6241.
23. Liu, Y.; Tang, Z. Multifunctional Nanoparticle@MOF Core–Shell Nanostructures. *Adv. Mater.* **2013**, *25*, 5819–5825.
24. Guo, S.; Wang, E. Noble Metal Nanomaterials: Controllable Synthesis and Application in Fuel Cells and Analytical Sensors. *Nano Today* **2011**, *6*, 240–264.
25. Garcia, M. A. Surface Plasmons in Metallic Nanoparticles: Fundamentals and Applications. *J. Phys. D: Appl. Phys.* **2011**, *44*, 283001.
26. Tao, A. R.; Habas, S.; Yang, P. Shape Control of Colloidal Metal Nanocrystals. *Small* **2008**, *4*, 310–325.
27. Xia, Y.; Xiong, Y.; Lim, B.; Skrabalak, S. E. Shape-Controlled Synthesis of Metal Nanocrystals: Simple Chemistry Meets Complex Physics? *Angew. Chem., Int. Ed.* **2009**, *48*, 60–103.
28. Cao, G.; Liu, D. Template-Based Synthesis of Nanorod, Nanowire, and Nanotube Arrays. *Adv. Colloid Interface Sci.* **2008**, *136*, 45–64.

29. Wang, C.; deKrafft, K. E.; Lin, W. Pt Nanoparticles@Photoactive Metal−Organic Frameworks: Efficient Hydrogen Evolution *via* Synergistic Photoexcitation and Electron Injection. *J. Am. Chem. Soc.* **2012**, *134*, 7211–7214.
30. Lim, D.-W.; Yoon, J. W.; Ryu, K. Y.; Suh, M. P. Magnesium Nanocrystals Embedded in a Metal−Organic Framework: Hybrid Hydrogen Storage with Synergistic Effect on Physi- and Chemisorption. *Angew. Chem., Int. Ed.* **2012**, *51*, 9814–9817.
31. He, L.; Liu, Y.; Liu, J.; Xiong, Y.; Zheng, J.; Liu, Y.; Tang, Z. Core−Shell Noble-Metal@Metal-Organic-Framework Nanoparticles with Highly Selective Sensing Property. *Angew. Chem., Int. Ed.* **2013**, *52*, 3741–3745.
32. Li, G.; Kobayashi, H.; Taylor, J. M.; Ikeda, R.; Kubota, Y.; Kato, K.; Takata, M.; Yamamoto, T.; Toh, S.; Matsumura, S.; *et al*. Hydrogen Storage in Pd Nanocrystals Covered with a Metal−Organic Framework. *Nat. Mater.* **2014**, *13*, 802–806.
33. Zhao, M.; Deng, K.; He, L.; Liu, Y.; Li, G.; Zhao, H.; Tang, Z. Core−Shell Palladium Nanoparticle@Metal−Organic Frameworks as Multifunctional Catalysts for Cascade Reactions. *J. Am. Chem. Soc.* **2014**, *136*, 1738–1741.
34. Morris, W.; Volosskiy, B.; Demir, S.; Gándara, F.; McGrier, P. L.; Furukawa, H.; Cascio, D.; Stoddart, J. F.; Yaghi, O. M. Synthesis, Structure, and Metalation of Two New Highly Porous Zirconium Metal−Organic Frameworks. *Inorg. Chem.* **2012**, *51*, 6443–6445.
35. Wang, Z.; Bharathi, M. S.; Hariharaputran, R.; Xing, H.; Tang, L.; Li, J.; Zhang, Y.-W.; Lu, Y. pH-Dependent Evolution of Five-Star Gold Nanostructures: An Experimental and Computational Study. *ACS Nano* **2013**, *7*, 2258–2265.
36. Murphy, P. J.; LaGrange, M. S. Raman Spectroscopy of Gold Chloro-Hydroxy Speciation in Fluids at Ambient Temperature and Pressure: A Re-evaluation of the Effects of pH and Chloride Concentration. *Geochim. Cosmochim. Acta* **1998**, *62*, 3515–3526.
37. Heasman, D. M.; Sherman, D. M.; Ragnarsdottir, K. V. The Reduction of Aqueous Au^{3+} by Sulfide Minerals and Green Rust Phases. *Am. Mineral.* **2003**, *88*, 725–739.
38. Harrach, G.; Valicsek, Z.; Horváth, O. Water-Soluble Silver(II) and Gold(III) Porphyrins: The Effect of Structural Distortion on the Photophysical and Photochemical Behavior. *Inorg. Chem. Commun.* **2011**, *14*, 1756–1761.
39. Antipas, A.; Dolphin, D.; Gouterman, M.; Johnson, E. C. Porphyrins. 38. Redox Potentials, Charge Transfer Transitions, and Emission of Copper, Silver, and Gold Complexes. *J. Am. Chem. Soc.* **1978**, *100*, 7705–7709.
40. Zhang, X.; Fu, L.; Liu, J.; Kuang, Y.; Luo, L.; Evans, D. G.; Sun, X. Ag@Zinc-Tetraphenylporphyrin Core-Shell Nanostructures with Unusual Thickness-Tunable Fluorescence. *Chem. Commun.* **2013**, *49*, 3513–3515.
41. Ohyama, J.; Hitomi, Y.; Higuchi, Y.; Shinagawa, M.; Mukai, H.; Kodera, M.; Teramura, K.; Shishido, T.; Tanaka, T. One-Phase Synthesis of Small Gold Nanoparticles Coated by a Horizontal Porphyrin Monolayer. *Chem. Commun.* **2008**, 6300–6302.
42. Dulkeith, E.; Morteani, A. C.; Niedereichholz, T.; Klar, T. A.; Feldmann, J.; Levi, S. A.; van Veggel, F. C. J. M.; Reinhoudt, D. N.; Möller, M.; Gittins, D. I. Fluorescence Quenching of Dye Molecules near Gold Nanoparticles: Radiative and Nonradiative Effects. *Phys. Rev. Lett.* **2002**, *89*, 203002.